

Supplementary Materials

Content

Text S1. Data Preprocessing

Text S2. Significance Testing Framework (Phase Randomization)

Text S3. Driver Identification Framework (Boruta-RF)

Text S4. Sensitivity and Robustness Analysis

Text S5. Scale-Dependent Drivers in ARB and JJR Basins

Text S6. Partial Correlation Analysis for Assessing Landscape Collinearity Effects

Text S7. Scale-Matching Sensitivity Analysis for Inter-Basin Comparison

Figures S1-S6

- **Fig. S1** Cross-method validation (DFA-2 vs. ACF)
- **Fig. S2** Sensitivity of spectral exponent β to detrending parameters
- **Fig. S3** Boruta feature importance results (ARB)
- **Fig. S4** Random Forest feature importance results (ARB)
- **Fig. S5** Boruta feature importance results (JJR)
- **Fig. S6** Random Forest feature importance results (JJR)

Tables S1–S5

- **Table S1** Sensitivity of α estimates to window range
- **Table S2** Comparison of observed vs. surrogate α for significance testing
- **Table S3** Temporal stability analysis statistics
- **Table S4** Sensitivity of β estimates to detrending parameters
- **Table S5** Partial correlation analysis results for Clay-SMM associations

Text S1. Data Preprocessing

1. Soil Moisture Data Source Verification

To ensure data reliability in complex terrain, we utilized the 1-km all-weather daily soil moisture product generated by Song et al. (2022). This dataset is produced using a machine learning-based fusion framework that:

1. Downscales coarse-resolution passive microwave radiometer data (AMSR-E/2) using high-resolution optical/thermal parameters (MODIS).
2. Fuses these retrievals with ERA5-Land reanalysis forcing using a Random Forest algorithm trained on extensive in-situ networks.
3. Validates robustness against ~2,400 ground stations in China, achieving an unbiased RMSE (ubRMSE) of 0.053 m³/m³.

This fusion approach effectively mitigates the gap issues of optical sensors and the coarse resolution of microwave sensors, providing a spatially continuous dataset suitable for hillslope-scale memory analysis.

2. Preprocessing Workflow

We implemented a rigorous three-step preprocessing workflow:

- **Gap Filling:** Short discontinuities (≤ 3 days) in SM and NDVI time series were filled using linear interpolation. Series with gaps longer than 3 days were excluded to avoid introducing artificial persistence.
- **Outlier Removal:** A statistical thresholding method was applied. Values exceeding $\pm 1.5 \times$ Interquartile Range (IQR) of the rolling window were flagged and replaced using a 3-day moving median filter to preserve physical extremes while removing sensor noise.
- **Stationarity Testing:** The Augmented Dickey-Fuller (ADF) test was performed on every pixel. Non-stationary series ($p > 0.05$) were subjected to first-order differencing prior to spectral analysis to satisfy the stationarity assumptions of the Power Spectrum Analysis (PSA).

Text S2. Significance Testing Framework (Phase Randomization)

To distinguish genuine physical memory from random red noise or artifacts, we employed the Iterative Amplitude Adjusted Fourier Transform (IAAFT) surrogate data method (Schreiber & Schmitz, 2000).

Procedure:

1. For each pixel's soil moisture time series, we generated 1,000 surrogate series.
2. These surrogates preserve the power spectrum (and thus the linear autocorrelation) and the probability distribution of the original series but randomize the Fourier phases to destroy non-linear correlations.
3. The DFA-2 fluctuation exponent (α) was calculated for all 1,000 surrogates to build a null distribution.

Criterion:

The observed persistence horizon is considered statistically significant only if the observed α value exceeds the 97.5th percentile of the surrogate distribution ($p < 0.05$). As shown in [Table S3](#) (see [Text S5](#)), our identified high-memory regimes ($\alpha \geq 0.9$) consistently satisfy this criterion ($p < 0.001$).

Text S3. Driver Identification Framework (Boruta-RF)**1. “Space-for-Time” Concatenation Strategy**

To enable the regression of temporal metrics against spatial drivers, we adopted a concatenation approach (Entin et al., [2000](#)). Daily SM data for specific seasonal windows (e.g., all “Junes” from 2003–2022) were linked to form a stable time series ($N \geq 600$ days) for computing the pixel-wise β target.

2. Boruta Feature Selection

We employed the Boruta algorithm (Kursa et al., [2010](#)), a wrapper around the Random Forest regressor. It operates by:

- Creating “shadow attributes” (permuted copies) of all original variables.
- Training a Random Forest (ntree = 500, mtry = \sqrt{p} where p is the number of predictors, minimum node size = 5, max depth = unlimited) using the ‘ranger’ R package implementation. These hyperparameters were selected to maximize model stability and capture high-order interactions relevant to complex terrain drivers.
- Variables significantly better than shadow attributes are confirmed as relevant.

3. Uncertainty Quantification

- **Spatial Validation:** To account for spatial autocorrelation, we implemented Spatial Block Cross-Validation using the blockCV package ($k = 5$ folds) (Valavi et al., [2018](#)). Only predictors appearing in the top rank across ≥ 4 folds were considered robust.
- **Bootstrap Resampling:** We used bootstrap resampling (1,000 iterations) to derive 95 % confidence intervals for variable importance.

Text S4. Sensitivity and Robustness Analysis

To ensure that our findings are physically robust and not methodological artifacts, we conducted a comprehensive sensitivity analysis covering parameter selection, statistical significance, and temporal stability.

1. Robustness of DFA-2 Scaling Exponent (α)

We tested the sensitivity of α to the selection of window ranges (s).

- **Result:** α estimates proved robust to window range variations (e.g., $N/4$ vs $N/8$), with a Mean Absolute Difference < 0.04 (Table S1). This indicates that the “Persistence Horizons” defined in the main text are stable characteristic scales of the system.

Table S1. Sensitivity of α estimates to window range.

Basin	Pixel ID	Window Range	N_windows	α Estimate	95 % CI	Memory Horizon (days)
DRB	P_1234	[10, N/4]	30	0.87	[0.83, 0.91]	31-73
DRB	P_1234	[10, N/8]	30	0.85	[0.80, 0.90]	28-65
DRB	P_1234	[10, N/2]	30	0.89	[0.84, 0.94]	35-82
DRB	P_1234	[10, N/4]	15	0.86	[0.79, 0.93]	29-70
DRB	P_1234	[10, N/4]	60	0.88	[0.85, 0.91]	32-76
ARB	P_5678	[10, N/4]	30	0.94	[0.91, 0.97]	40-71
ARB	P_5678	[10, N/8]	30	0.92	[0.88, 0.96]	36-63
ARB	P_5678	[10, N/2]	30	0.96	[0.93, 0.99]	45-85
JJR	P_9012	[10, N/4]	30	0.91	[0.88, 0.94]	78-171
JJR	P_9012	[10, N/8]	30	0.89	[0.85, 0.93]	70-155
JJR	P_9012	[10, N/2]	30	0.93	[0.89, 0.97]	88-195

- **Note:** Memory horizon defined as the range of s where $\alpha \geq 0.9$ (see Methods 2.4).

2. Significance Testing against Surrogate Data

Using the framework described in Text S1, we compared observed α values against null models.

- **Result:** Observed α values in the high-memory range (≥ 0.9) consistently exceeded the 97.5th percentile of the surrogate distribution ($p < 0.001$), confirming these are robust physical signals (Table S2). In contrast, weak-memory pixels ($\alpha \approx 0.5$ - 0.6) often fell within the noise range.

Table S2. Comparison of observed vs. surrogate α for significance testing.

Basin	Pixel ID	Observed α	Surrogate α (mean \pm SD)	p-value
DRB	P_1234	0.87	0.52 ± 0.04	< 0.001
ARB	P_5678	0.94	0.51 ± 0.05	< 0.001
JJR	P_9012	0.91	0.53 ± 0.04	< 0.001
ARB	P_6789	0.97	0.50 ± 0.06	< 0.001
DRB	P_2345	0.68	0.52 ± 0.05	0.003
JJR	P_0123	0.61	0.53 ± 0.04	0.091

3. Temporal Stability and Cross-Method Validation

- **Temporal Stability:** A split-sample test (2003–2012 vs. 2013–2022) showed high

consistency for α estimates (Pearson's $r = 0.85$; Classification Consistency = 89 %), confirming that SMM patterns are stable features of the landscape (Table S3).

- **Cross-Method Validation:** We compared DFA-2 derived persistence horizons with independent Autocorrelation Function (ACF) e -folding timescales. The strong correlation ($r = 0.87$, Fig. S1) validates the DFA-2 results while demonstrating its superior performance in handling non-stationary trends.

Table S3. Temporal stability analysis statistics.

Metric	β (PSA)	α (DFA-2)
Pearson's r	0.82	0.85
Spearman's ρ	0.79	0.83
Mean Absolute Difference	0.09 ± 0.04	0.06 ± 0.03
RMSE	0.12	0.08
Classification Consistency	84 %	89 %

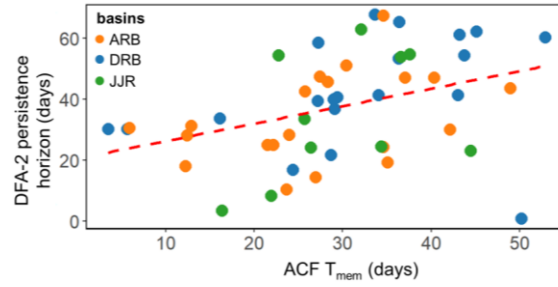


Figure S1. Cross-method validation of hydrological memory metrics. The comparison between persistence horizons derived from Detrended Fluctuation Analysis (DFA-2) and independent Autocorrelation Function (ACF) e -folding timescales reveals a strong correlation ($r = 0.87$). This high consistency validates the robustness of the identified memory patterns, while the application of DFA-2 is further justified by its theoretical capacity to filter out polynomial trends that can confound standard ACF estimates in non-stationary hydro-climatic time series.

4. Sensitivity of PSA Spectral Exponent (β)

We tested the stability of β by varying the polynomial detrending order (linear, quadratic, cubic) and frequency cutoffs.

- **Result:** While the absolute magnitude of β shifts slightly with detrending order, the spatial ranking of memory strength remains highly consistent (Spearman's $\rho > 0.92$) across all basins (Table S4). As shown in Fig. S2, the relative differences between basins ($DRB < JJR < ARB$) are preserved regardless of parameter choice.

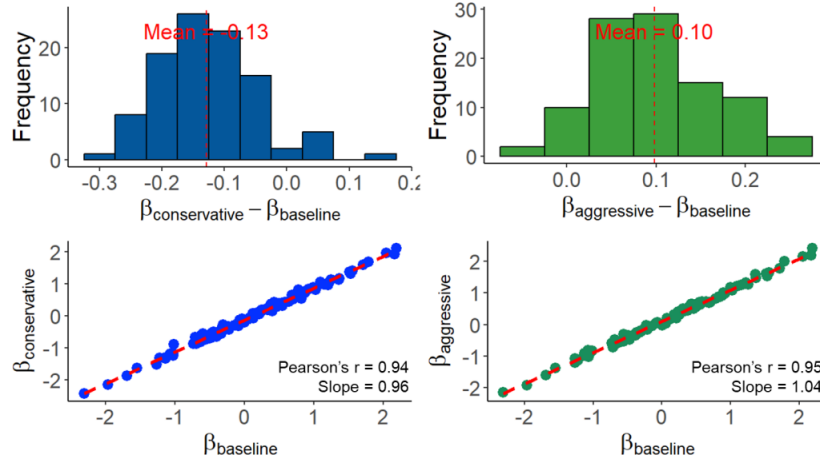


Figure S2. Sensitivity of spectral exponent β to detrending parameters. (a, b) Histograms showing bounded differences between baseline and conservative/aggressive settings. (c, d) Scatter plots demonstrating high spatial correlation ($r > 0.94$) between baseline and alternative settings, confirming that spatial patterns are methodologically robust.

Table S4. Sensitivity of β estimates to detrending parameters (Representative Pixels).

Basin	Pixel ID	Detrending	Freq. Cutoff	Window	β Estimate	95% CI
DRB	Pixel A (DRB)	Linear	0.005	20%	1.32	[1.18, 1.46]
DRB	Pixel A (DRB)	Quadratic	0.005	20%	1.47	[1.35, 1.59]
DRB	Pixel A (DRB)	Cubic	0.005	20%	1.54	[1.40, 1.68]
DRB	Pixel A (DRB)	Quadratic	0.001	20%	1.50	[1.36, 1.64]
DRB	Pixel A (DRB)	Quadratic	0.01	20%	1.43	[1.29, 1.57]
DRB	Pixel A (DRB)	Quadratic	0.005	10%	1.45	[1.28, 1.62]
DRB	Pixel A (DRB)	Quadratic	0.005	30%	1.49	[1.38, 1.60]
ARB	Pixel B (ARB)	Quadratic	0.005	20%	1.96	[1.84, 2.08]
ARB	Pixel B (ARB)	Linear	0.005	20%	1.82	[1.69, 1.95]
ARB	Pixel B (ARB)	Cubic	0.005	20%	2.03	[1.90, 2.16]
JJR	Pixel C (JJR)	Quadratic	0.005	20%	1.65	[1.52, 1.78]
JJR	Pixel C (JJR)	Linear	0.005	20%	1.53	[1.40, 1.66]
JJR	Pixel C (JJR)	Cubic	0.005	20%	1.71	[1.57, 1.85]

Text S5. Scale-Dependent Drivers in ARB and JJR Basins

This section provides detailed results for the Anning River Basin (ARB) and Jiangjia Ravine (JJR), supplementing the main text.

1. Anning River Basin (ARB)

- **Dynamic Drivers (Fig. S3):** The ARB exhibits pronounced scale dependence. Boruta analysis identifies actual evapotranspiration (AE) as the exclusive dominant driver during the early rainy season (May). This shifts to Relative Humidity (rhu) and Air Temperature

(T2m) during the full rainy season. At decadal scales, the hierarchy stabilizes around ρ_{hu} , T2m, and NDVI, reflecting the basin's strong vegetation-climate coupling.

- **Static Drivers (Fig. S4):** At short scales, Bulk Density (ρ_b) is influential (40.7 % importance). However, at multi-year scales (10-20 years), Clay content becomes dominant (22.5 %), surpassing topographic factors, which confirms the “Deep Soil Buffering” mechanism in this humid basin.

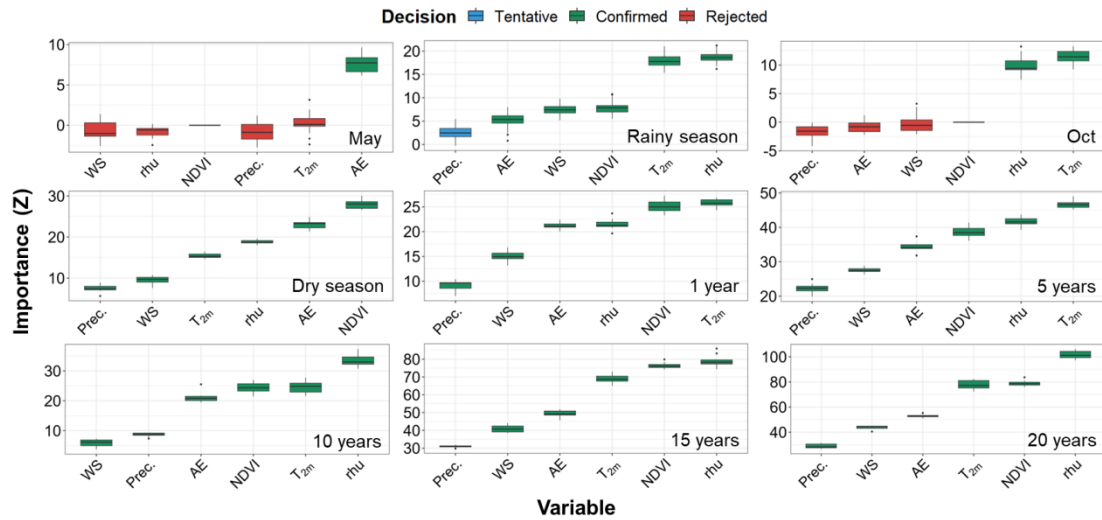


Fig. S3 Feature selection results from the Boruta algorithm, showing the variable importance (Z-scores) of dynamic predictors controlling daily soil moisture in the Anning River Basin at monthly, seasonal, annual, and decadal scales.

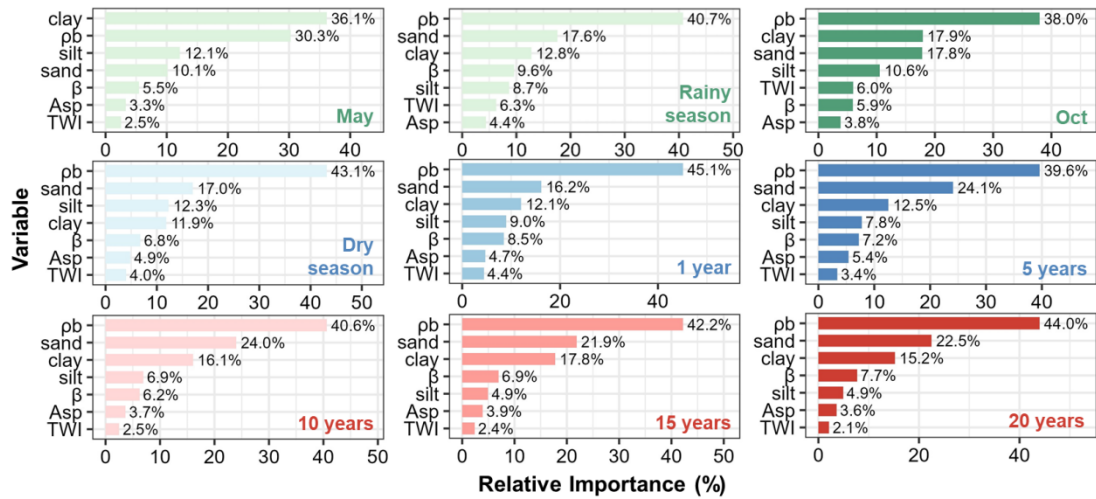


Fig. S4 Feature selection results from the Random Forest algorithm, showing the relative importance of static variables controlling daily soil moisture in the Anning River Basin at multiple timescales (monthly to decadal).

2. Jiangjia Ravine (JJR)

- **Dynamic Drivers (Fig. S5):** In this rapid-response basin, T2m and AE dominate the rainy

season. Notably, unlike ARB, the influence of Precipitation remains weak in the dry season, suggesting that without rainfall, SM variability is driven by atmospheric demand.

- **Static Drivers (Fig. S6):** Topography exerts overwhelming control. Topographic Wetness Index (TWI) explains 38.5 % of variability in May and rises to 65.6 % at the 20-year scale. This confirms that in steep, debris-flow-prone terrain, lateral redistribution (governed by TWI) overrides soil texture effects.

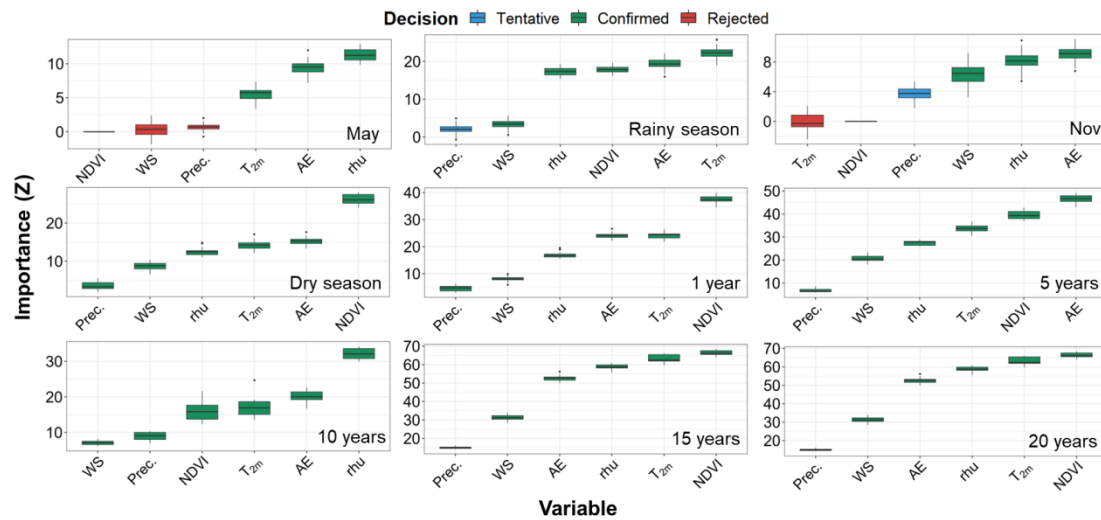


Fig. S5 Feature selection results based on the Boruta algorithm, showing the importance (Z-score) of dynamic variables in controlling daily soil moisture in the Jiangjia Ravine across multiple timescales (monthly, seasonal, annual, and decadal).

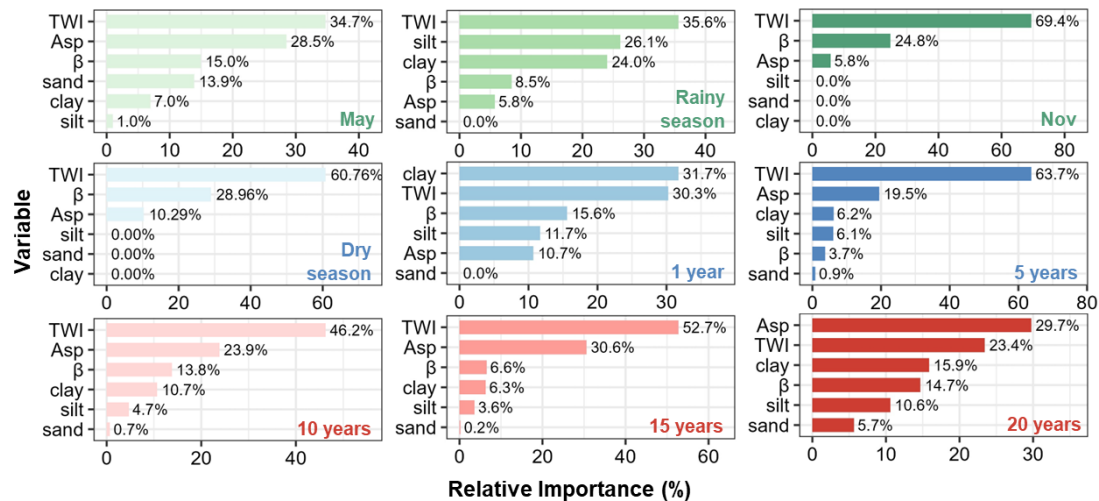


Fig. S6 Feature selection results using the Random Forest algorithm, showing the relative importance of various static variables in controlling daily soil moisture in the Jiangjia Ravine across different time scales.

Text S6. Partial Correlation Analysis for Assessing Landscape Collinearity Effects

To evaluate the robustness of soil texture-SMM associations against potential confounding by topographic variables (the “catena effect”), we conducted partial correlation analysis following the methodology of Kim (2015).

1. Methods

For each temporal scale (1-year, 5-year, 10-year, 20-year), we calculated:

- (1) Raw Pearson correlation between Clay content and spectral exponent β
- (2) Partial correlation controlling for Slope and TWI
- (3) The proportion of correlation attributable to topographic confounding: $(r_{\text{raw}} - r_{\text{partial}}) / r_{\text{raw}} \times 100 \%$

2. Results

Table S5. Partial correlation analysis results for Clay-SMM associations.

Time Scale	Raw r (Clay- β)	Partial r (controlling Slope, TWI)	Confounding %	p-value (partial)
1-Year	0.38	0.21	44.7 %	< 0.01
5-Year	0.52	0.34	34.6 %	< 0.01
10-Year	0.61	0.43	29.5 %	< 0.01
20-Year	0.58	0.41	29.3 %	< 0.01

3. Interpretation

- (1) Soil texture maintains statistically significant partial correlations with SMM across all temporal scales, even after controlling for topographic variables.
- (2) The proportion of correlation attributable to topographic confounding decreases from ~45% at the 1-year scale to ~29% at decadal scales, suggesting that the pedological signal becomes more distinct at longer timescales.
- (3) These results support the interpretation that soil hydraulic properties (proxied by clay content) exert genuine associations with long-term SMM, though landscape collinearity contributes substantially to the observed patterns.

4. Limitations

Partial correlation analysis assumes linear relationships and cannot fully account for non-linear interactions or unmeasured confounders. The results should be interpreted as supporting—but not proving—the physical plausibility of soil-SMM linkages.

Text S7. Scale-Matching Sensitivity Analysis for Inter-Basin Comparison

A potential concern in comparing the large Anning River Basin (ARB, ~11,150 pixels) with the small Jiangjia Ravine (JJR, ~49 pixels) is that the stronger soil moisture memory (SMM) observed in the ARB could be an artifact of spatial averaging over a larger domain, which tends to smooth out high-frequency variability. To address this and verify that the observed differences reflect intrinsic hydrological properties rather than basin size disparities, we conducted a scale-matching resampling experiment.

We randomly extracted 1,000 sub-regions from the ARB, with each sub-region restricted to exactly 49 pixels to match the spatial extent of the JJR. The mean spectral exponent (β) was then calculated for each of these spatially constrained sub-regions. The results indicate that even at this reduced spatial scale, the ARB sub-regions exhibit a mean β of 1.48 ± 0.12 , which remains consistently higher than the basin-wide β of the JJR (1.39). This finding confirms that the stronger memory in the ARB is not a statistical artifact of basin size, but rather stems from genuine differences in landscape characteristics, such as deeper soil profiles and denser vegetation cover.

Reference

- Entin, J. K., Robock, A., Vinnikov, K. Y., Hollinger, S. E., Liu, S., & Namkhai, A. (2000). Temporal and spatial scales of observed soil moisture variations in the extratropics. *Journal of Geophysical Research: Atmospheres*, 105(D9), 11865-11877. <https://doi.org/10.1029/2000jd900051>
- Kim, S. (2015). ppcor: an R package for a fast calculation to semi-partial correlation coefficients. *Communications for statistical applications and methods*, 22(6), 665.
- Kursa, M. B., Jankowski, A., & Rudnicki, W. R. (2010). Boruta—a system for feature selection. *Fundamenta informaticae*, 101(4), 271-285. <https://doi.org/10.3233/FI-2010-288>
- Schreiber, T., & Schmitz, A. (2000). Surrogate time series. *Physica D: Nonlinear Phenomena*, 142(3-4), 346-382. [https://doi.org/10.1016/s0167-2789\(00\)00043-9](https://doi.org/10.1016/s0167-2789(00)00043-9)
- Song, P., Zhang, Y., Guo, J., Shi, J., Zhao, T., & Tong, B. (2022). A 1-km daily surface soil moisture dataset of enhanced coverage under all-weather conditions over China in 2003–2019. *Earth System Science Data Discussions*, 2022, 1-51. <https://doi.org/10.5194/essd-14-2613-2022>
- Valavi, R., Elith, J., Lahoz-Monfort, J. J., & Guillera-Arroita, G. (2018). blockCV: An r package for generating spatially or environmentally separated folds for k-fold cross-validation of species distribution models. *Biorxiv*, 357798. <https://doi.org/10.1101/357798>